# A Digital Approach to via Edge Roughness Characterization and Quantification

Kuan Lu<sup>1</sup> · Pengfei Lin<sup>1</sup> · ChaBum Lee<sup>1</sup>

Received: 2 April 2024 / Revised: 18 June 2024 / Accepted: 24 June 2024 / Published online: 5 July 2024 © Korean Society for Precision Engineering 2024

#### **Abstract**

This paper presents an innovative digital integration combining edge diffractometry with convolutional neural networks (CNN) for via metrology and inspection. The beam propagation method (BMP) was applied to simulate the edge diffractometry-generated interferogram for via edge roughness ( ) characterization, and a comprehensive database that correlated distinct fringe patterns to VER was further established for CNN training. The well-trained CNN-based methodology provided a fast and accurate VER assessment with a root mean squared error (RMSE) of 0.073 and an average mean absolute deviation ratio (MADR) of 2.274%. In addition, the proposed digital approach was compared with the multilayer perceptron machine (MLP) in terms of computational efficiency and predictive accuracy. The proposed digital integration significantly improved the accuracy and speed of VER measurement, characterization, and quantification, potentially enhancing device yield and reliability. The successful application of this digital approach could pave the way for various types of via or pattern metrology.

Keywords Via, Via edge roughness, Metrology; Inspection; Interferogram; Artificial intelligence; Convolutional Neural Networks.

# 1 Introduction

Via metrology and inspection technology are vital to verify that the vias produced through machining, laser drilling, or chemical etching meet their designated specifications such as diameter, circularity, roundness, and edge roughness conditions [1]. The via technology enabled the 3D stacked chips for low power consumption, performance [2], which is also essential for signal transmission and the overall performance of the devices [3]. The dimension and shape accuracy of the vias is important since performance degradation or complete failure of the whole device could result from small discrepancies [4]. Similar to the line-edge roughness (LER) of the photomask patterns, the VER is also vital to ensure the reliability of the system, since the rough edges could lead to increased electron scattering, affecting the conductivity and cause variations in the electrical characteristics [5]. Currently, various via-measuring methods are utilized to perform the measurements. Optical microscopy

With the advancement of artificial intelligence (AI), Convolutional Neural Networks (CNNs) can automatically conduct feature extraction from images and predict performance of semiconductor component [9]. With the aid of big data technology and Industry 4.0 [10], various manufactured data will be continuously collected and stored, making the training sets more comprehensive. Thus, the robustness and reliability of CNN will further be enhanced over time [11]. However, the majority of deep learning-based methods are applied at wafer level. There are only a few studies that have applied deep learning for TSV inspection and quality evaluation. Current research mainly focuses on the detection of TSV extrusion, overall performance evaluation, and the dimension prediction of TSVs, including array alignment and critical dimensions [9,12-14]. To our best knowledge, the application of deep-learning for edge roughness characterization, which is a very challenging metrology task, has not been developed yet.



is a widely used via inspection method, providing rapid assessment of size and shape, but its ability is limited for deep or small vias [6]. Scanning electron microscopy (SEM) and atomic force microscopy (AFM) enable detailed analysis of via edge roughness and its microstructure, but both methods are expensive and time-consuming, making them unsuitable for in-process inspection [7,8].

<sup>☑</sup> Dr. ChaBum Lee cblee@tamu.edu

J. Mike Walker '66 Department of Mechanical Engineering, Texas A&M University 3123 TAMU, College Station, TX 77843-3123, USA

Inspired by previous studies [15-17], numerical optical simulation and CNN were integrated to automate via edge roughness characterization. By analyzing various via diffractive patterns and their corresponding VER, the CNN can automatically extract subtle patterns from these fringe images, and further correlate those features with roughness metrics. Thus, the well-trained model can directly predict the roughness from the diffraction pattern, enabling an accurate and fast via metrology and inspection. Instead of utilizing a simplified aperture diffraction model in previous studies, the beam propagation method (BPM) was applied to simulate the fringe patterns generated from the vias. In this paper, details of dataset construction and digital approaches to via characterization are explained, and the potential to be integrated into existing via inspection frameworks is also discussed.

# 2 Framework of the Digital Approach

Fig. 1 compares the flow charts of the proposed digital via inspection approach to the AS-IS hole metrology method. Instead of conducting complicated fringe preprocessing [17], a well-trained CNN model is capable of predicting the edge roughness condition from the diffraction image directly.

CNN is widely used in computer vision and image processing since it simulates the cognitive pattern of the human brain [18], being successfully applied in various industrial scenarios [19,20]. In this study, the cropped diffraction image served as input and predicted VER values

were the output.

The proposed digital approach consists of two major steps: the first step involves the establishment of a database that links distinct fringe patterns with their corresponding edge roughness conditions. The second step focuses on the setup of neural networks, including the training of models and optimization of hyperparameters. Details of each step will be discussed in the following sections.

# 3. Establishment of the Training Database

# 3.1 Experiments Setup

A grayfield through silicon via (TSV) inspection system was constructed as shown in Fig. 2(a), which features enhanced sensitivity to scattered light and remarkable diffractive image contrast. A collimated laser ( $\lambda$  450 nm) was utilized as the light source. The laser was further shaped into a donut shape by the two axicon lenses installed below it, as depicted in Fig. 2(b). To reduce the intensity saturation in the imaging device, a 12.5% neutral density (ND) filter was applied. The filtered donut-shaped beam was then formed into a spherical wavefront through the first objective lens. Once the light interacted with the edge of the TSV, the Charge-coupled Device (CCD) on the bottom could capture the diffraction images. In this study, all diffraction images were captured from  $\phi$ 100  $\mu$ m TSVs fabricated on 210  $\mu$ m thick undoped single-crystalline silicon wafers.

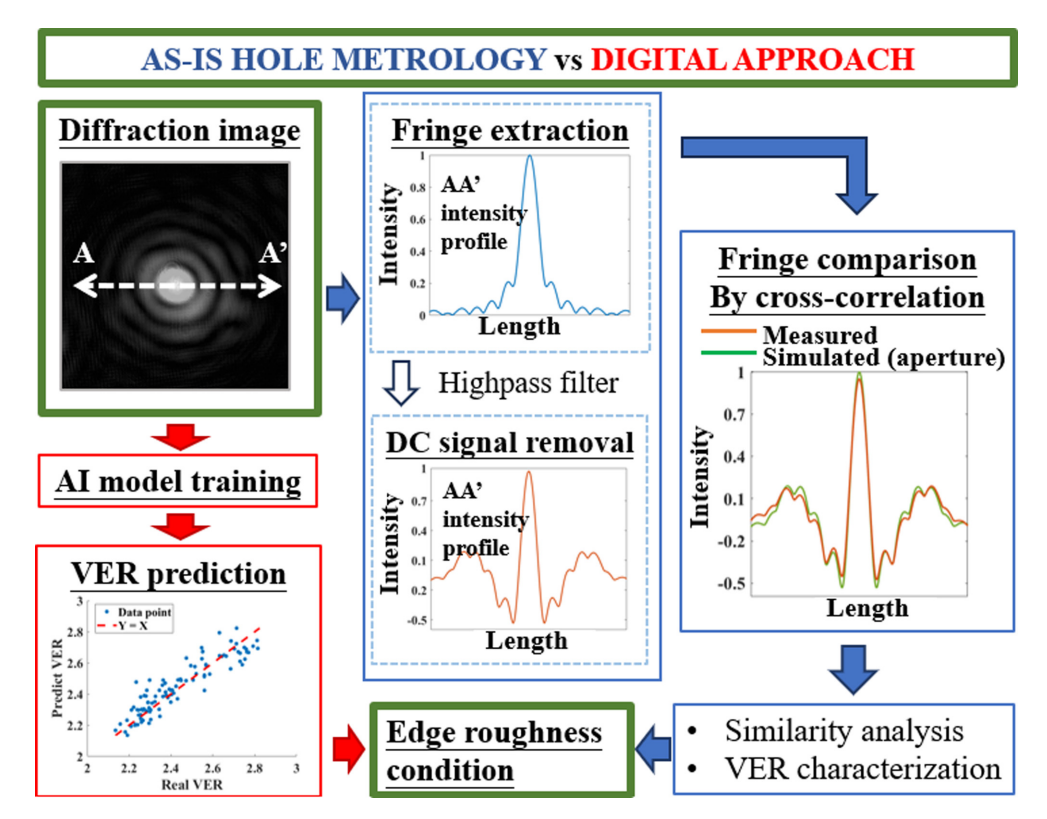


Fig. 1 Comparison between AI-based digital approach and AI-IS hole inspection method

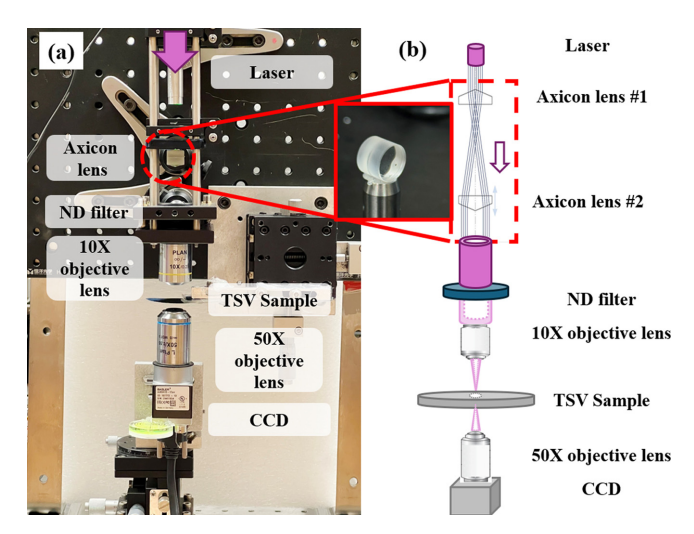


Fig. 2 Schematics of grayfield Si-via inspection system

#### 3.2 Simulation Model

The BPM was used to simulate the laser propagation inside the via sample. This method is widely applied for simulating electromagnetic (EM) wave propagation through waveguides [21,22] and other devices and media, such as waveguide junctions [23], optical switches [24], optical fiber amplifiers [25] and atmosphere with turbulence [26]. The BPM assumes that the envelope of the optical wave would not change abruptly during the propagation [23]. Therefore, the transverse electrical field density of the optical wave traveling in z-direction is represented as:

$$E_t = \Psi_t e^{-in_0 k_0 z} \tag{1}$$

where  $\Psi_t$  is the Slowly Varying Envelope (SVE) function,  $n_0$  is the reference refractive index, and  $k_0$  is the wave number of the laser in the vacuum.

By substituting this expression into the Maxwell equation and applying the paraxial approximation, the governing equation for a scalar wave propagation can be written as [23]:

$$2in_0k_0\frac{\partial \Psi_t}{\partial z} = \frac{\partial^2 \Psi_t}{\partial x^2} + \frac{\partial^2 \Psi_t}{\partial y^2} + k_0^2(n^2 - n_0^2)\Psi_t$$
 (2)

where n is the refractive index of the media. After giving the initial condition  $\Psi_t(z=0) = \Psi_0(x,y)$ , the  $\Psi_t$  could be solved for each z value by finite difference method in the alternative direction implicit (ADI) scheme. In this study, the initial condition was set as the Bessel-Gaussian function to represent the laser beam generated by passing a Gaussian beam through a pair of axicon lenses [27,28]:

$$\Psi_{t}(\rho, z=0) = A_{m} \exp\left[-\frac{\rho^{2}}{w_{o}^{2}}\right] J_{m}(\sqrt{a}\rho)$$
(3)

where  $w_0$  is the size of the beam waist,  $\rho = \sqrt{x^2 + y^2}$  is the polar coordinate,  $A_m$ , m and  $\sqrt{a}$  are constant values. By choosing different combinations of  $w_0$ ,  $A_m$ , m and  $\sqrt{a}$ , various types of laser beams, including Gaussian beam and Donut-Beam, could

be represented.

The simulation of BPM started and ended at the top (z = 0) and bottom (z = h) of via sample, respectively. Once the field value  $U_0(x,y) = \Psi_t(z=h) \cdot e^{-in_0k_0h}$  was obtained at the bottom, the scalar diffraction theory was used to compute the diffraction pattern received by the CCD. The expression for computing the diffraction filed after propagating a distance Z is written as [29]:

$$U_2(x,y) = \Im^{-1} \{ \Im \{ U_0(x,y) \} e^{jkz} \exp[-j\pi\lambda Z (f_y^2 + f_y^2)] \}$$
 (4)

where  $\mathfrak{I}$  and  $\mathfrak{I}^{-1}$  are Fourier transform and inverse Fourier transform,  $f_X$  and  $f_Y$  are frequency variables associated with x and y respectively. The diffraction pattern on the CCD could be computed as [29]:

$$I(x,y) = |U_2(x,y)|^2$$
 (5)

where I(x,y) represents the irradiance of the light field, which is the time-averaged radiometric energy flux per unit area.

# 3.3 Training Set Preparation

Fig. 3 depicts the workflow of training datasets processing. After the acquisition of diffraction patterns through interferogram, image segmentation was conducted in a 10-degree interval. Subsequently, the measured diffraction pattern of each segment was extracted and compared to the BPM simulation fringe in ideal condition to obtain the similarity value (SI). Diffraction fringes of multiple edge conditions with different VER values were further simulated using BPM methods, which was used to compared with the ideal fringe. Thus, the relationship between VER and SI was obtained, and this calibration result was used to estimate the VER of experimental fringe pattern. This method was described in detail in a previous work [17].

After performing the same operation on each fringe segment, a dataset containing diffractive images and its associated VER was established, consisting of 1,872 entries total. The dataset served as input for training the CNN model, aiming for accurate edge roughness prediction based on precise pattern recognitions. In this study, five experiments were conducted: in each experiment, 100 samples were randomly selected as the testing set while the remaining 1,772 samples served as training sets.

### 3.4 Model Optimization

In order to improve the prediction accuracy and obtain the best CNN model, the hyperparameters, including the number and properties of different types of layers, were optimized in this study. Both perdition accuracy (RMSE and MADR) and computational burden (training time) were taken into consideration for choosing the best model. The final architecture of the CNN is shown in Fig. 4, which consists of 2 convolutional layers, 2 max-pooling layers, and 1 fully connected dense layer. In corresponding sub boxes of Fig. 4, @ denotes the number of feature maps, and × represents the

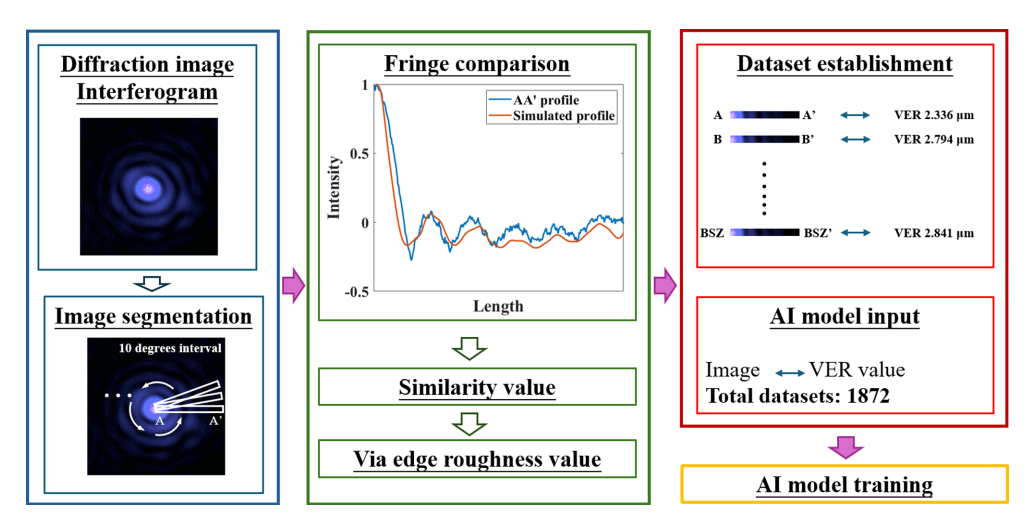


Fig. 3 Schematics of the establishment of training datasets

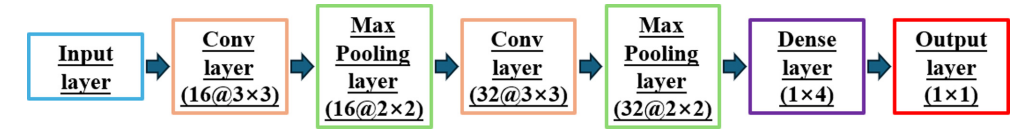


Fig. 4 The final architecture of the CNN model

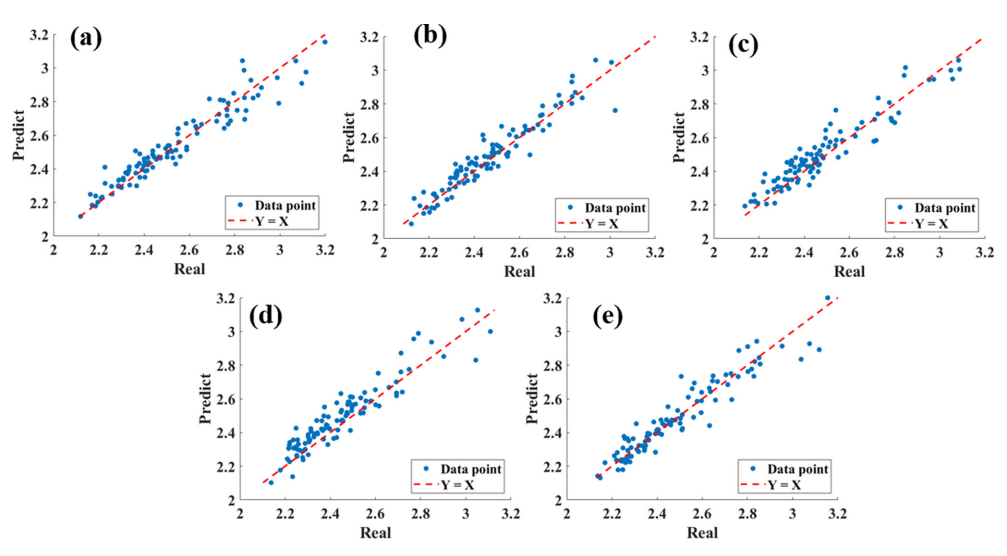


Fig. 5 Predicted vs actual scatter plot results of five datasets

dimensions of the filter or pooling window. During the training process, the adaptive learning rate strategy was applied to reduce the training time needed to reach convergence.

### 4. Results

### **4.1 CNN Prediction Results**

Fig. 5 shows the CNN prediction results of five experiments, allowing an intuitive evaluation of its performance. In each subplot, the blue points represented the relationship between the actual value and CNN's predicted value, while the red dashed line represented the ideal prediction scenario where the

predicted value equaled the actual value (Y = X). These charts visualized the prediction accuracy: the closer the data points were to the red line, the higher the accuracy of the predictions. As shown in Fig. 5, in all five scenarios, blue points were scattered in a region close to the red reference line along the whole VER range, indicating the CNN model was capable of making relatively precise VER predictions.

Two evaluation metrics were further used to numerically evaluate the results: the root mean square error (RMSE), and the mean absolute deviation ratio (MADR) which is computed as mean absolute deviation divided by average. The average RMSE for all testing sets was 0.073, with the first and second sets having values less than 0.069 while the highest, 0.082, was from the fourth set. Considering the average VER was



Fig. 6 The final architecture of the MLP model

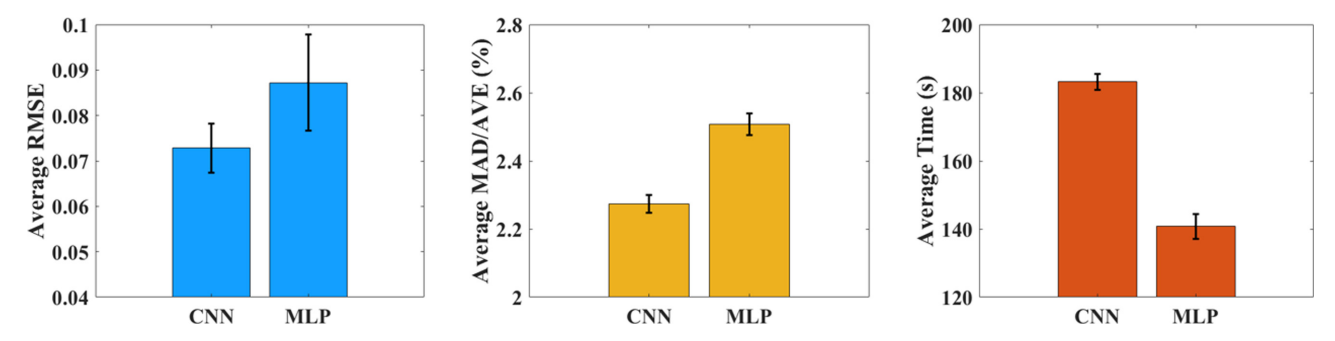


Fig. 7 Result comparisons: (a) average RMSE, (b) average MADR, and (c) average training time

more than  $2.480 \, \mu m$ , all RMSEs were considered relatively small and reflected the precision of the predictions. Upon further calculation of the MADR, the average value obtained was only 2.274%, with the fourth set having the highest value at just 2.767%. This further demonstrated that CNN's average predictive error is below 2.300%, being considered highly accurate.

# 4.2 Additional Multilayer Perceptron (MLP) Results

The MLP, also a neural network-based model, is widely used to solve classification and prediction problems [30-32]. In the MLP model, all the layers, including the input, hidden, and output layers, are fully connected layers [33]. As shown in Fig. 6, the MLP consists of one input layer, one output layer and 4 hidden layers. The hyper parameters of the MLP were also tuned through a 10-fold cross-validation for achieving the best performance. This relatively simple model structure can make the model training and prediction process more efficient by reducing the number of parameters. However, this smaller number of parameters limits the model's capability for complicated tasks such as complicated image and video processing [34].

A comprehensive comparison of the prediction accuracy and computation time between CNN and MLP was conducted, as shown in Fig. 7. From the results, CNN showed a significant advantage in prediction accuracy: with a lower average RMSE and a better MADR. The average RMSE of MLP results was 0.0872, 19.78% higher than that of CNN. Similarly, the average MADR results for MLP was 2.507%, 10.249% higher than that of CNN. In semiconductor industry, the TSVs provide electrical connection among multiple layers, even a small increase in VER could result in attenuation and distortion of the signal being transferred, due to the skin effect. Therefore, a small difference in prediction performance can have huge impacts in engineering practice.

However, due to the simpler network structure of MLP,

23.144% less training time was needed, making it a more efficient inspection method in industrial applications. It is noteworthy that by comparing the standard deviation, CNN showed a more robust predictive performance, while MLP's performance was significantly influenced by the training sets itself.

The choice between utilizing CNN or MLP should be guided by the specific industrial requirements, depending on whether the priority lies with achieving the highest accuracy possible or with efficiency and speed of computation.

#### **5 Conclusion**

Through integration of experimental and theoretical edge diffractometry with CNN, a novel digital approach to automatic via metrology and inspection was proposed in this paper. The electromagnetic wave propagation-based computational model of the via created a database of simulated fringe profiles, the experiment by the grayfield edge diffractometry was conducted to obtain the fringe pattern dataset to further compute VER. The CNN model was then trained to analyze various via diffractive profiles and their corresponding VER, automatically extracting subtle patterns from these fringe images. A further correlation between the fringe image features and VER showed the linear characteristics.

The proposed CNN-based digital approach showed a 0.073 RMSE and a 2.274% MADR in VER prediction results, proving its capacity in complex fringes analysis, offering a robust solution for the semiconductor industry's demand for rapid and precise via inspection. An additional study on an MLP-based model offered a trade-off between prediction efficiency and accuracy.

In summary, the implementation of the proposed digital approach in via metrology is promised to improve the yield and reliability of semiconductor devices, further supporting the technological advancements in the industry. Future research could focus on further optimizing the AI models and exploring potential applications in other areas of precision engineering.

**Author's Contribution** All authors equally contributed to this study: design, experiment, and data analysis.

**Acknowledgment** This research has been supported by the National Science Foundation (CMMI #212499).

**Data Availability** The data that supports the findings of this study are available from the corresponding author upon reasonable request.

**Disclosures** The authors declare no conflicts of interest.

## References

- Alapati, R., Travaly, Y., Van Olmen, J., Teixeira, R. C., Vaes, J., van Cauwenbergh, M., Jourdain, A., Verbinnen, G., Marcucilli, G., Florence, G., Wolfling, S., Pelissier, C., Zhang, H., Sinha, J., Machura, A., & Malik, I. (2009). TSV metrology and inspection challenges. *Proceedings of the 2009 IEEE International* Conference on 3D System Integration, 1-4.
- Lu, M. C. (2022). Advancement of chip stacking architectures and interconnect technologies for image sensors. *Journal of Electronic Packaging*, 144(2), 020801.
- Dong, G, Biao, Y., Xidong, D., & Yuan, L. (2017). Research on the influence of vias on signal transmission in multi-layer PCB. Proceedings of the 2017 13th IEEE International Conference on Electronic Measurement & Instruments (ICEMI), 406-409.
- Persson, E., Eriksson, I., & Zackrisson, L. (1997). Effects of hole machining defects on strength and fatigue life of composite laminates. Composites Part A: Applied Science and Manufacturing, 28(2), 141-151.
- Duan, S., Zhang, Z., Wei, K., Wang, F., & Han, X. (2020). Theoretical study and physical tests of circular hole-edge stress concentration in long glass fiber reinforced polypropylene composite. *Composite Structures*, 236, 111884.
- Liao, H.-C., Lim, Z.-Y., Hu, Y.-X., & Tseng, H.-W. (2018).
   Guidelines of automated optical inspection (AOI) system development. Proceedings of the 2018 IEEE 3rd International Conference on Signal and Image Processing (ICSIP), 362-366.
- Kaspar, J., Luft, A., Nolte, S., Will, M., & Beyer, E. (2006). Laser helical drilling of silicon wafers with ns to fs pulses: Scanning electron microscopy and transmission electron microscopy characterization of drilled through-holes. *Journal of Laser Applications*, 18(2), 85-92.
- Bayat, P., Vogel, D., Rodriguez, R. D., Sheremet, E., Zahn, D. R. T., Rzepka, S., & Michel, B. (2015). Thermo-mechanical characterization of copper through-silicon vias (Cu-TSVs) using micro-Raman spectroscopy and atomic force microscopy. *Microelectronic Engineering*, 137, 101-104.
- Kim, J., Kim, S., Kwon, N., Kang, H., Kim, Y., & Lee, C. (2018).
   Deep learning based automatic defect classification in through-silicon via process: Fa: Factory automation. *Proceedings of the 2018 29th Annual SEMI Advanced Semiconductor Manufacturing Conference (ASMC)*, 35-39.

- 10. Popkova, E. G., Ragulina, Y. V., & Bogoviz, A. V. (2019). Industry 4.0: Industrial revolution of the 21st century. *Springer*.
- 11. Ding, N., & Möller, K. (2022). Robustness evaluation on different training state of a CNN model. *Current Directions in Biomedical Engineering*, 8(2), 497-500.
- Jalilvand, G., Lindsay, J., Reidy, B., Shukla, V., Duggan, D., Zand, R., & Jiang, T. (2021). Application of machine learning in recognition and analysis of TSV extrusion profiles with multiple morphology. *Proceedings of the 2021 IEEE 71st Electronic* Components and Technology Conference (ECTC), 1652-1659).
- 13. Kim, K., Park, H., Lho, D., Kim, M., Son, K., Son, K., Kim, S., Shin, T., Choi, S., & Kim, J. (2020). Deep reinforcement learning-based through silicon via (TSV) array design optimization method considering crosstalk. *Proceedings of the 2020 IEEE Electrical Design of Advanced Packaging and Systems (EDAPS)*, 1-3.
- Li, J.-W., Su, E., & Ho, C.-C. (2024). Prediction of critical dimensions for 3D TSV structures using artificial neural network. *Metrology, Inspection, and Process Control XXXVIII, 12955*, 649-653.
- Lu, K., Wang, Z., Chun, H., & Lee, C. (2023). Curved-edge diffractive fringe pattern analysis for wafer edge metrology and inspection. *Proceedings of the Metrology, Inspection, and Process Control XXXVII*, 12496, 105-106. https://doi.org/10.1117/ 12.2665016
- Wang, Z., Lu, K., & Lee, C. (2023). A fringe pattern analysis technique for photomask line-edge-roughness characterization. Proceedings of the International Manufacturing Science and Engineering Conference, 87240, V002T06A007.
- 17. Lu, K., & Lee, C. (2024). Hole Edge Metrology and Inspection by Edge Diffractometry. *Journal of Manufacturing Science and Engineering*, 146(7), 070905.
- 18. Goodfellow, I., Bengio, Y., & Courville, A. (2016). Deep learning. *The MIT press*.
- Kim, I. S., Lee, M. G., & Jeon, Y. (2023). Review on machine learning based welding quality improvement. *International Journal* of *Precision Engineering and Manufacturing-Smart Technology*, 1(2), 219-226.
- Shin, H., Ahn, J., Beak, S. W., & Lee, S. W. (2024). Development of 1D-convolutional neural network-based height profile prediction model in directed energy deposition process using melt-pool image data. *International Journal of Precision Engineering and Manufacturing-Smart Technology*, 2(1), 57-65.
- 21. Raghuwanshi, S. K., & Palodiya, V. (2016). Beam propagation and mode coupling study in a coupled waveguide structure by using scalar finite element method. *Optik*, 127(3), 1237-1244.
- 22. Masanori, K. (2014). Optical waveguide theory by the finite element method. *Springer Dordrecht*.
- 23. Pedrola, G. L. (2015). Beam propagation method for design of optical waveguide devices. *John Wiley & Sons*.
- Wu, Y.-D. (2005). All-optical logic gates by using multibranch waveguide structure with localized optical nonlinearity. *IEEE Journal of Selected Topics in Quantum Electronics*, 11(2), 307-312.
- Jauregui, C., Eidam, T., Limpert, J., & Tünnermann, A. (2011).
   Impact of modal interference on the beam quality of high-power fiber amplifiers. *Optics express*, 19(4), 3258-3271.

- Chahine, Y. K., Tedder, S. A., Vyhnalek, B. E., & Wroblewski, A. C. (2020). Beam propagation through atmospheric turbulence using an altitude-dependent structure profile with non-uniformly distributed phase screens. *Proceedings of the Free-Space Laser Communications XXXII*, 11272, 263-277. https://doi.org/10.1117/12.2543583
- Dallaire, M., McCarthy, N., & Piché, M. (2009). Spatiotemporal bessel beams: theory and experiments. *Optics Express*, 17(20), 18148-18164.
- Dickey, F. M. (2018). Laser beam shaping: theory and techniques. CRC press. Voelz, D. (2011). Computational Fourier Optics: A MATLAB Tutorial. SPIE.
- 29. Voelz, D. (2011). Computational Fourier Optics: A MATLAB Tutorial. *SPIE*.
- Amani, S., Lee, J. B., & Park, S. S. (2023). Prediction of spread in steel wire rod rolling: transferable and explainable approach. *International Journal of Precision Engineering and Manufacturing-Smart Technology, 1*(1), 19-33.
- Kim, S., Kim, Y., Sugita, N., & Mitsuishi, M. (2023). Surface assessment of transparent glass plate with wavelength-modulated interferometry and harmonic phase-iterative method. *International Journal of Precision Engineering and Manufacturing-Smart Technology*, 1(1), 71-81.
- 32. Chae, S., & Bae, S. (2024). Bayesian hyper-parameter optimization in one-dimensional convolutional autoencoder for monitoring bearing health status. *International Journal of Precision Engineering and Manufacturing-Smart Technology, 2*(1), 15-22.
- 33. Avuçlu, E., & Başçiftçi, F. (2018). New approaches to determine age and gender in image processing techniques using multilayer perceptron neural network. *Applied Soft Computing*, 70, 157-168.
- Desai, M., & Shah, M. (2021). An anatomization on breast cancer detection and diagnosis employing multi-layer perceptron neural network (MLP) and Convolutional neural network (CNN), *Clinical* eHealth, 4, 1-11.